Tactile-Guided Auxiliary Manipulation of Leafy Branches for Robotic Pruning

Yuseung Jo, *Graduate Student Member, IEEE*, Yonghyun Park, Sechang Lee, Tapomayukh Bhattacharjee, and Hyoung Il Son, *Senior Member, IEEE*

***Abstract*—Robotic pruning in dense agricultural canopies is limited by visual detection of the target branch and by physical access to the intended cutting region. In manual pruning, obstructive branches are often pushed aside while the hand regulates contact using tactile cues associated with local pressure and deformation. Motivated by this interaction principle, this letter presents a tactile-guided framework for displacing and holding leafy branches using sparse capacitive feedback. A three-module capacitive tactile array mounted on the auxiliary manipulator provides normalized pressure- or indentation-sensitive intensity signals, which are converted into a contact-center surrogate, a tactile directional cue, and a rate-weighted moment cue for tactile-guided Cartesian control. The framework uses these tactile quantities as local control cues, without reconstructing full plant geometry or estimating a calibrated contact wrench. A four-condition comparison comprises 384 attempted manipulations on eight real leafy branches from two source plants. Marker-measured stem displacement and holding variation are evaluated alongside tactile-response exposure and actual arrival time. Paired comparisons identify condition- and branch-dependent effects of the motion corrections.**

***Index Terms*—Robotics and automation in agriculture and forestry, agricultural automation, robotics and automation in life sciences.**

Received 13 May 2026; accepted 24 October 2026. Date of publication 10 November 2026; date of current version 20 November 2026. This article was recommended for publication by Associate Editor Z. Wang and Editor H. Moon upon evaluation of the reviewers' comments. This work was supported by the Korea Institute of Planning and Evaluation for Technology in Food, Agriculture and Forestry (IPET) through the AX-Based Intelligent Agricultural Work Collaboration Industrialization Technology Development Program, funded by the Ministry of Agriculture, Food and Rural Affairs (MAFRA) under Grant RS-2026-25519039. *(Corresponding author: Hyoung Il Son.)*

Yuseung Jo and Sechang Lee are with the Department of Convergence Biosystems Engineering, Chonnam National University, Gwangju 61186, Republic of Korea, and also with Interdisciplinary Program in IT-Bio Convergence System, Chonnam National University, Gwangju 61186, Republic of Korea (e-mail: ysjo68@jnu.ac.kr; 190612@jnu.ac.kr).

Yonghyun Park is with the Physical-AI Operated Locomotion and Autonomous Robotics in Extreme Environments (POLAR-AI) Research Center, Gwangju Institute of Science and Technology (GIST), Gwangju 61005, Republic of Korea, and also with Research Center for Biological Cybernetics, Chonnam National University, Gwangju 61186, Republic of Korea (e-mail: parkoh25@gist.ac.kr).

Tapomayukh Bhattacharjee is with the Department of Computer Science, Cornell University, Ithaca, NY 14853 USA (e-mail: tapomayukh@cornell.edu).

Hyoung Il Son is with the Department of Convergence Biosystems Engineering, Chonnam National University, Gwangju 61186, Republic of Korea, also with the Interdisciplinary Program in IT-Bio Convergence System, Chonnam National University, Gwangju 61186, Republic of Korea, and also with Research Center for Biological Cybernetics, Chonnam National University, Gwangju 61186, Republic of Korea (e-mail: hison@jnu.ac.kr).

This article has supplementary downloadable material available at https://doi.org/10.1109/LRA.2026.3752004, provided by the authors.

Digital Object Identifier 10.1109/LRA.2026.3752004

I. Introduction

During manual pruning, a supporting hand can displace and hold surrounding foliage while the other hand operates a cutting tool. Local tactile information helps regulate such contact through cues related to deformation and pressure [1], [2], [3]. Robotic harvesting and pruning systems have advanced visual localization and approach execution [4], [5], [6]. These capabilities motivate complementary auxiliary manipulation to displace and hold leafy branches (Fig. 1).

During a push, a leaf can fold against the tactile array or slide across it while the supporting stem moves very little. The array measures contact at the tool, whereas the task is to displace a selected stem and hold it there. Tool travel and peak tactile response alone therefore give incomplete evidence of task success. Prior work has used tactile feedback to advance through foliage while limiting canopy disturbance [7]. Here, displacement of the contacted branch is the intended outcome. We ask whether the distribution and timing of local contact provide useful motion corrections beyond the slowing that peak intensity alone can supply.

Sparse tactile sensing is attractive in agricultural manipulation, where compliance, wiring, and calibration constrain sensor design [8]. With just three capacitive modules, two contact patterns can produce the same peak reading on opposite sides of the array. An intensity-based controller would impose the same forward-speed limit in both cases, although the readings contain different directional information.

1) We formulate a tactile feedback law for displacing and holding a leafy branch. Peak channel response limits forward speed, while the spatial distribution of the three readings corrects translation and a rate-weighted moment about the array center corrects rotation.
2) We quantify the incremental effects of translational and rotational correction through paired controller comparisons under a common nominal reference for each branch. Independent stem markers measure displacement and holding variation, which we assess alongside tactile exposure and arrival time.

II. Related Work

A. Robotic Pruning and Agricultural Manipulation

Pruning and harvesting robots localize targets, estimate plant geometry, and plan approaches [5], [9], [10], [11], [12], [13].

2377-3766 © 2026 IEEE. All rights reserved, including rights for text and data mining, and training of artificial intelligence and similar technologies. Personal use is permitted, but republication/redistribution requires IEEE permission. See https://www.ieee.org/publications/rights/index.html for more information.

Authorized licensed use limited to: CHONNAM NATIONAL UNIVERSITY. Downloaded on November 22,2026 at 10:55:00 UTC from IEEE Xplore. Restrictions apply.

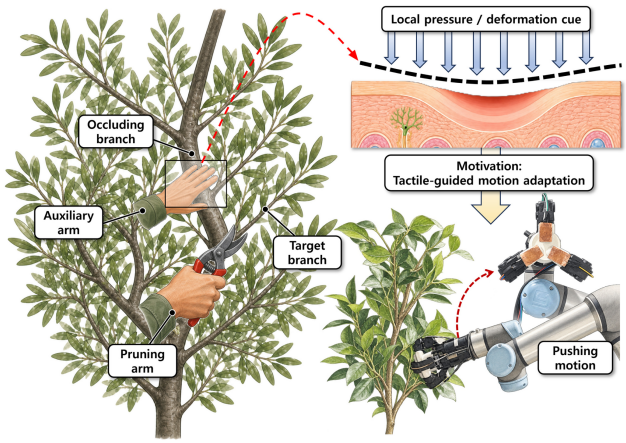


Fig. 1. Tactile-guided auxiliary manipulation: manual pruning motivates displacing surrounding vegetation, local pressure and deformation motivate tactile regulation, and the wrist-mounted array guides robotic pushing of leafy branches.

Multiarm systems coordinate crop handling [14], [15], [16], HortiBot uses force–torque sensing for compliant contact [17], and scene graphs guide agricultural task and arm selection [18].

B. Tactile Sensing for Contact-Rich Manipulation

Tactile feedback supports grasping [19], [20], [21], local perception and servoing [22], [23], learned manipulation [24], [25], [26], [27], and interaction with articulated objects [28]. We use three existing CushSense modules [29] to guide motion during foliage contact.

C. Plant Interaction and Research Positioning

Robots rearrange clutter by push-grasping [30], planning around movable obstacles [31], [32], mechanical search [33], and tactile actions that relieve jamming [34]. In canopies, Push Past Green moves foliage to reveal occluded space [35]. RICE uses spatial and temporal tactile cues to reach a target while limiting canopy disturbance, and tracks branch motion [7].

Our objective is to displace and hold a selected stem. We compare tactile corrections under the same branch-specific reference, without a direct performance comparison to either prior system.

A robot can reach its commanded pose by folding leaves against the stem while the stem barely moves. Conversely, a policy that limits disturbance to surrounding foliage may be effective for reaching a target, even when the selected stem scarcely moves. We therefore compare controllers using displacement measured by markers on the selected stem.

III. Problem Formulation and Notation

A. Auxiliary Leafy-Branch Manipulation Task

An operator selects a leafy branch and specifies a nominal motion of the tool center point (TCP) to displace and hold it through leaf or stem contact. Robotic pruning motivates this auxiliary task.

The fixed unit vector $\mathbf{n} \in \mathbb{R}^3$, $\|\mathbf{n}\| = 1$, specifies the nominal pushing direction in the robot base frame. Stem displacement is an independently measured outcome, not a prescribed control reference.

B. Notation and Control Variables

The transform $\mathbf{T}_a(t) \in SE(3)$ maps the TCP frame to the robot base frame, with position $\mathbf{x}_a(t) \in \mathbb{R}^3$ and rotation $\mathbf{R}_a(t) \in SO(3)$. Measured and commanded base-frame twists are $\boldsymbol{\xi}_a = \left[\mathbf{v}_a^\top \ \boldsymbol{\omega}_a^\top\right]^\top$ and $\boldsymbol{\xi}_{\text{cmd}}$. The three modules have known planar locations $\mathbf{p}_i \in \mathbb{R}^2$ and normalized readings $\bar{I}_i \in [0,1]$; locations and planar cues use the tactile-plane frame.

The local tactile state is represented by

$$\mathcal{S}_t = \left\{ A(t), \hat{\mathbf{c}}(t), \tilde{P}_s(t), \mathbf{e}_P(t), \tilde{M}_z(t) \right\}, \tag{1}$$

where maximum response $A(t) = \max_i \bar{I}_i(t)$ limits forward motion, $\hat{\mathbf{c}}$ is a contact-center surrogate, $\tilde{P}_s$ and $\mathbf{e}_P$ give directional-cue magnitude and direction, and $\tilde{M}_z$ is a rate-weighted moment cue. Vector-derived $\tilde{P}_s$ can be small through cancellation even when A is high; it is not pressure in pascals.

The nominal auxiliary position and orientation references are denoted by $\mathbf{x}_d(t)$ and $\mathbf{R}_d(t)$, respectively. The positive-part operator is defined as $[a]_+ = \max(a, 0)$.

C. Assumptions and Scope

The three sensor locations are known, coplanar, and non-collinear. Channel readings are referenced to unloaded values and corrected for polarity and scale. Under distributed contact, the cues provide neither a unique contact point nor a calibrated wrench. CushSense can be calibrated for normal force [29]; this controller uses normalized responses.

The operator supplies the reference shared by all variants for each branch. Branch detection, cutting-point selection, tool clearance, and coordinated cutting lie outside the evaluation.

IV. Tactile Contact-Cue Estimation

The estimated center provides a geometric reference for the directional and moment cues used in Section V. It is not a Cartesian target.

A. Contact-Center Surrogate

The inputs $\bar{I}_i \in [0,1]$ are channel readings conditioned using unloaded references, response polarity, scaling, smoothing, and clipping. The channel settings and cue scales are shared across the compared conditions.

The normalized intensity is mapped to a distance surrogate:

$$d_i(t) = \max\left\{0, \alpha_i - \beta_i \bar{I}_i(t)\right\}, \quad \alpha_i > 0, \ \beta_i > 0. \tag{2}$$

The fixed coefficients α_i, β_i share the coordinate unit of $\mathbf{p}_i$; d_i decreases with response but is not measured distance. For $\hat{\mathbf{c}} = [\hat{c}_x, \hat{c}_y]^\top$, subtracting the first circle relation $\|\hat{\mathbf{c}} - \mathbf{p}_i\|^2 = d_i^2$ from the other two gives $\mathbf{A}\hat{\mathbf{c}} = \mathbf{b}$, with

$$\begin{aligned} \mathbf{A}_{j,:} &= 2(\mathbf{p}_{j+1} - \mathbf{p}_1)^\top, \\ b_j &= d_1^2 - d_{j+1}^2 + \|\mathbf{p}_{j+1}\|^2 - \|\mathbf{p}_1\|^2, \\ \hat{\mathbf{c}}(t) &= \mathbf{A}^\dagger \mathbf{b}(t), \qquad j = 1, 2. \end{aligned} \tag{3}$$

Authorized licensed use limited to: CHONNAM NATIONAL UNIVERSITY. Downloaded on November 22,2026 at 10:55:00 UTC from IEEE Xplore. Restrictions apply.

Here $\mathbf{A}^{\dagger}$ denotes the Moore–Penrose pseudoinverse. The original circle constraints need not intersect, so this solution remains a surrogate under distributed contact. Below the contact threshold on all channels, tactile corrections are zero.

B. Contact Direction and Moment Cue

Bearing vectors are defined as

$$\mathbf{r}_i = \hat{\mathbf{c}} - \mathbf{p}_i, \quad \mathbf{v}_i = \frac{\mathbf{r}_i}{\|\mathbf{r}_i\| + \epsilon_r}. \tag{4}$$

Here $\epsilon_r > 0$ has the same coordinate unit as $\mathbf{r}_i$, so $\mathbf{v}_i$ is dimensionless. The intensity-weighted tactile-cue vector is

$$\mathbf{q}_p(t) = \sum_{i=1}^{3} \bar{I}_i(t)\mathbf{v}_i(t). \tag{5}$$

For feedback, this vector is separated into tactile-response magnitude and direction:

$$\tilde{P}_s(t) = \min\left(1, \frac{\|\mathbf{q}_p(t)\|}{P_{\text{scale}}}\right), \quad \mathbf{e}_P(t) = \frac{\mathbf{q}_p(t)}{\|\mathbf{q}_p(t)\| + \epsilon_q}, \tag{6}$$

The dimensionless scale $P_{\text{scale}} > 0$ and regularizer $\epsilon_q > 0$ are fixed across conditions. Clipping bounds $\tilde{P}_s$ in [0,1], while $\mathbf{e}_P$ tends to zero with $\mathbf{q}_p$ and need not have unit norm. The cue angle $\hat{\theta} = \text{atan2}([\mathbf{e}_P]_y, [\mathbf{e}_P]_x)$ is defined only for sufficient magnitude; it is not plant orientation. When channel contributions oppose one another, their vector sum can decrease despite substantial individual readings. Directional correction then weakens, while the independently retained maximum A can still activate the forward-motion limit.

To retain spatially asymmetric changes in the channel cues, define the fixed array center $\mathbf{c}_0 = \frac{1}{3}\sum_i \mathbf{p}_i$ and moment arms $\boldsymbol{\rho}_i = \mathbf{p}_i - \mathbf{c}_0$. With $\mathbf{f}_i(t) = \bar{I}_i(t)\mathbf{v}_i(t)$,

$$m_i(t) = [\boldsymbol{\rho}_i \times \mathbf{f}_i(t)]_z = \rho_{i,x} f_{i,y} - \rho_{i,y} f_{i,x}. \tag{7}$$

The rate weight and normalized moment cue are calculated as

$$\kappa_i(t) = \frac{\|\mathbf{f}_i(t) - \mathbf{f}_i(t - \Delta t)\|}{\Delta t},$$
$$\tilde{M}_z(t) = \text{clip}\left(\frac{\sum_{i=1}^{3} \kappa_i(t) m_i(t)}{M_{\text{scale}}}, -1, 1\right). \tag{8}$$

Here $\Delta t > 0$ is the sample interval. $M_{\text{scale}} > 0$ has the units of $\sum_i \kappa_i m_i$, making $\tilde{M}_z$ dimensionless. Signed cross products retain spatial asymmetry; nonnegative rate weights emphasize faster changes.

Rate history is reset after invalid timing or samples, and initialized to zero at contact entry. Using $\mathbf{r}_i$ as the moment arm would yield zero because $\mathbf{f}_i \parallel \mathbf{r}_i$. With fixed responses and geometry, rate weights vanish; symmetry can also cancel contributions. Residual noise affects the cue, which is not a calibrated torque or slip measurement.

V. Tactile-Guided Auxiliary Manipulation

At each update, the measured TCP state supplies nominal feedback and the measured orientation maps the tactile cues into the base frame. The controller sends the resulting linear and angular velocities as one twist.

A. Nominal Motion Reference

The nominal motion is specified by three operator-taught TCP positions: a noncontact start, a nominal contact point $\mathbf{x}_0$, and a pushing goal $\mathbf{x}_g$. The approach connects the start to the contact waypoint. With time measured from the start of the nominal pushing phase, the pushing reference is

$$\mathbf{x}_d(t) = \mathbf{x}_0 + s(t)\mathbf{n}, \quad 0 \le s(t) \le s_{\max}, \tag{9}$$

where $\mathbf{n} = (\mathbf{x}_g - \mathbf{x}_0)/\|\mathbf{x}_g - \mathbf{x}_0\|$, $s_{\max} = \|\mathbf{x}_g - \mathbf{x}_0\|$, and $s(t)$ is a smooth, velocity-limited displacement profile. The nominal orientation remains fixed at the taught orientation. All variants share the waypoints, reference time profile, and velocity and acceleration bounds within each branch. The contact waypoint is a spatial reference; foliage contact may begin before or after it. NT uses no tactile input for commands or phase transitions. The nominal Cartesian command is

$$\mathbf{v}_{\text{nom}} = \mathbf{K}_p(\mathbf{x}_d - \mathbf{x}_a) - \mathbf{K}_d\dot{\mathbf{x}}_a, \tag{10}$$

$$\boldsymbol{\omega}_{\text{nom}} = -\mathbf{K}_R\mathbf{e}_R^b - \mathbf{K}_\Omega\boldsymbol{\omega}_a,$$
$$\mathbf{e}_R^b = \mathbf{R}_d\text{Log}\left(\mathbf{R}_d^\top\mathbf{R}_a\right)^\vee. \tag{11}$$

The matrices $\mathbf{K}_p$ and $\mathbf{K}_R$ set position and orientation feedback, while $\mathbf{K}_d$ and $\mathbf{K}_\Omega$ set linear and angular velocity damping. $\text{Log}(\cdot)^\vee$ gives the relative rotation vector, mapped to the base frame by $\mathbf{R}_d$.

When the nominal reference reaches the goal, it remains there. Holding begins only after the measured TCP position remains within 3 mm of the goal for 0.20 s; orientation error is excluded from this arrival test. The pushing timeout is 20 s. During holding, each condition continues its control law with the same goal and original reference orientation, rather than resetting the reference to its actual arrival pose. The supplied schedule is therefore shared, but arrival time remains an outcome of execution.

B. Translational Correction and Intensity Limiting

The scaled tactile directional cue is mapped to the robot base frame:

$$\tilde{\mathbf{F}}^b = \tilde{P}_s\mathbf{R}_a\mathbf{P}_t\mathbf{e}_P, \tag{12}$$

where $\mathbf{P}_t \in \mathbb{R}^{3\times 2}$ embeds the orthonormal tactile-plane axes in the TCP frame. Using the measured $\mathbf{R}_a$, rather than the taught $\mathbf{R}_d$, keeps this mapping attached to the array as its orientation changes. With positive gain k_f, the translational correction and combined linear command are

$$\mathbf{v}_{\text{tac}} = -k_f\tilde{\mathbf{F}}^b,$$
$$\mathbf{v}_\Sigma = \mathbf{v}_{\text{nom}} + \mathbf{v}_{\text{tac}}. \tag{13}$$

This prescribed cue-to-motion mapping is not projected onto $\mathbf{n}$ and can produce lateral or backward correction. The gain k_f converts the dimensionless cue to linear velocity; $\tilde{\mathbf{F}}^b$ is not a physical reaction force.

Authorized licensed use limited to: CHONNAM NATIONAL UNIVERSITY. Downloaded on November 22,2026 at 10:55:00 UTC from IEEE Xplore. Restrictions apply.

The maximum response A independently limits positive progress along $\mathbf{n}$. Let $\bar{v}_+(A) \geq 0$ be the predetermined forward-speed ceiling, nonincreasing with A above the activation threshold A_{ctl}. Define

$$\mathcal{L}_A(\mathbf{v}) = \begin{cases} \mathbf{v} - \mathbf{n}\left[\mathbf{n}^\top \mathbf{v} - \bar{v}_+(A)\right]_+, & A > A_{\text{ctl}}, \\ \mathbf{v}, & A \leq A_{\text{ctl}}. \end{cases} \tag{14}$$

When active, $\mathbf{n}^\top \mathcal{L}_A(\mathbf{v}) = \min(\mathbf{n}^\top \mathbf{v}, \bar{v}_+(A))$, while $(\mathbf{I} - \mathbf{n}\mathbf{n}^\top)\mathcal{L}_A(\mathbf{v}) = (\mathbf{I} - \mathbf{n}\mathbf{n}^\top)\mathbf{v}$. Thus only excessive positive progress is removed from the combined command; lateral and backward components are preserved.

Common robot command processing maps $\mathbf{v}_\Sigma$ to $\mathbf{v}_{\text{pre}}$ before the final intensity-limit check. IO, Trans, and Full share this check and its settings, transmitting

$$\mathbf{v}_{\text{cmd}} = \mathcal{L}_A(\mathbf{v}_{\text{pre}}). \tag{15}$$

NT transmits $\mathbf{v}_{\text{pre}}$ directly. For tactile conditions the final check limits combined forward demand after smoothing, including nominal feedback. It does not bound contact force. Nominal tracking continues without contact.

C. Moment-Cue Correction and Execution

Let $\mathbf{e}_z^t$ be the normal axis of the tactile plane, and let $\mathbf{e}_z^b = \mathbf{R}_a \mathbf{e}_z^t$ be the corresponding base-frame direction. The angular tactile bias is

$$\boldsymbol{\omega}_{\text{tac}} = -k_m \tilde{M}_z \mathbf{e}_z^b. \tag{16}$$

The gain $k_m > 0$ maps the dimensionless moment cue to angular velocity about the tactile-plane normal. With a dimensionless threshold $M_{\max} > 0$, the angular attenuation is

$$\lambda_M = \text{clip}\left(1 - \frac{\left[|\tilde{M}_z| - M_{\max}\right]_+}{M_{\max}}, 0, 1\right), \tag{17}$$

and the angular command is

$$\boldsymbol{\omega}_{\text{cmd}} = \text{sat}_\Omega(\boldsymbol{\omega}_{\text{nom}} + \lambda_M \boldsymbol{\omega}_{\text{tac}}). \tag{18}$$

Within $|\tilde{M}_z| \leq 1$, λ_M is one up to $M_{\max}$, then decreases linearly to zero at $2M_{\max}$. It scales only the tactile term; sat_Ω bounds the combined angular command. The low-level controller receives $\boldsymbol{\xi}_{\text{cmd}} = [\mathbf{v}_{\text{cmd}}^\top \ \boldsymbol{\omega}_{\text{cmd}}^\top]^\top$.

All four conditions retain the nominal controller. No tactile (NT) sets $k_f = k_m = 0$ and bypasses $\mathcal{L}_A$. Intensity-only (IO) uses the same zero correction gains with $\mathcal{L}_A$ active. Translation-only (Trans) adds $k_f > 0$ while retaining $k_m = 0$. Proposed method (Full) retains the same linear settings and adds $k_m > 0$. "Translation-only" names the tactile correction: nominal orientation feedback remains active in every condition. Shared gains, cue scales, thresholds, and limits are fixed across the relevant comparisons.

Full–IO tests both corrections together. Trans–IO and Full–Trans test the successive additions of translation and rotation. These comparisons assess displacement empirically; the feedback law gives no convergence or optimality guarantee.

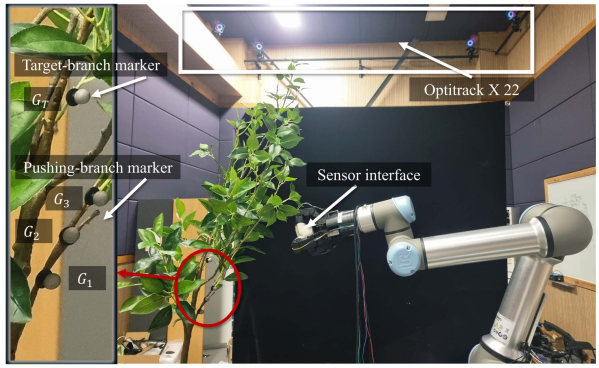


Fig. 2. Experimental setup and marker placement. A representative real-plant testbed with a UR5, three-module tactile array, and OptiTrack tracking (ten cameras in the room). The left inset shows proximal, middle, and distal markers G_1, G_2, G_3 on the manipulated stem and the target-branch marker G_T.

TABLE I
PLANT-TRIAL COMPLETION AND MEASUREMENT AVAILABILITY

Condition	Attempts	Hold complete	Valid D, H
NT	96	92	84
IO	96	91	84
Trans	96	96	91
Full	96	90	82

VI. EXPERIMENTS

We first characterize the contact cues, then compare all four controllers on a common set of plant trials.

A. Setup and Baselines

The UR5 carried a three-module CushSense array (Fig. 2). Each of two laboratory testbeds contained four selected branches, drawn from two source plants in total. OptiTrack measured stem motion independently at three equally spaced markers, G_1, G_2, G_3.

Within a branch, all four conditions shared the taught start, contact and goal positions, reference orientation, motion profile, and arrival and holding rules. Twelve four-condition blocks per branch yielded 384 attempts (Table I). The supplementary video shows plant trials.

The nominal pushing speed was 10 mm/s. Enabled tactile gains were $k_f = 0.003$ m/s and $k_m = 0.2$ rad/s, with $A_{\text{ctl}} = 0.65$.

Condition order was balanced within each branch: each condition occupied each of the four order positions three times.

B. Metrics

Marker positions $\mathbf{g}_i(t)$ and the unit pushing direction $\mathbf{n}$ are expressed in a common coordinate frame. Let $\mathbf{g}_i^0$ be the pre-push baseline and $\mathcal{H}$ the common-duration holding window after actual TCP arrival. The signed projected displacement and its spatial summary are

$$\delta_i(t) = \mathbf{n}^\top \left[\mathbf{g}_i(t) - \mathbf{g}_i^0\right],$$
$$D = \frac{\langle \delta_1 \rangle_{\mathcal{H}} + 2\langle \delta_2 \rangle_{\mathcal{H}} + \langle \delta_3 \rangle_{\mathcal{H}}}{4}. \tag{19}$$

Authorized licensed use limited to: CHONNAM NATIONAL UNIVERSITY. Downloaded on November 22,2026 at 10:55:00 UTC from IEEE Xplore. Restrictions apply.

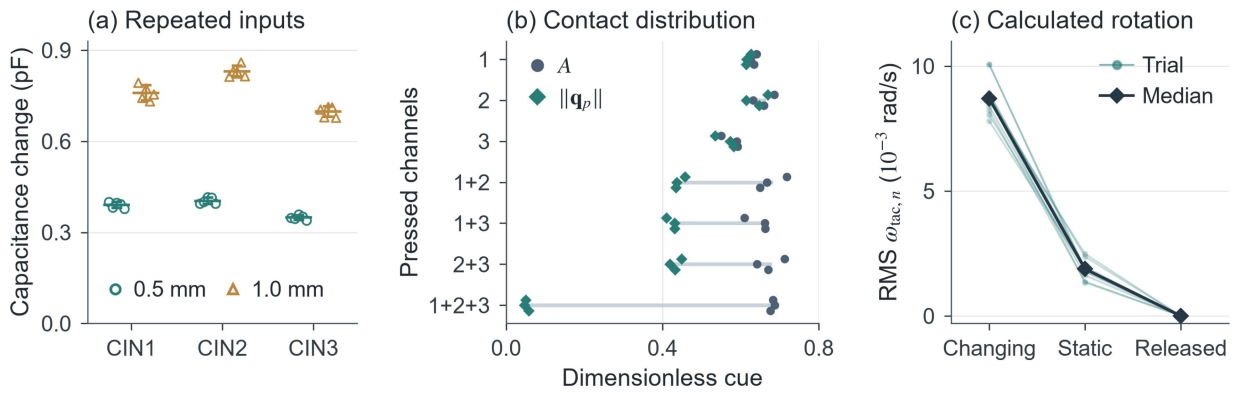


Fig. 3. Contact-cue characterization. (a) Trial plateau responses, with mean and standard deviation ($n = 5$ per channel and input). (b) Maximum response A and resultant magnitude $\|\mathbf{q}_p\|$: symbols are record means ($n = 3$ per pattern), connected by pattern means. (c) RMS of the calculated angular term; lines connect the same record ($n = 12$), diamonds show medians.

The normalized trapezoidal weights 1:2:1 approximate segment-average displacement across two equal inter-marker intervals. The proximal marker contributes even with smaller motion; signs are retained and the target-branch marker is not subtracted.

Holding variation is calculated for each marker before spatial aggregation:

$$h_i = Q_{0.95}(\delta_i \mid \mathcal{H}) - Q_{0.05}(\delta_i \mid \mathcal{H}),$$
$$H = (h_1 + 2h_2 + h_3)/4. \tag{20}$$

This order avoids cancellation between opposite marker motions. H includes drift and is not a three-dimensional pose error or a vibration-frequency measure.

For valid observed time $\mathcal{V}$ within the pushing phase, the high-response exposure and actual arrival time are

$$E_A = 100\,\frac{\int_{\mathcal{V}} \mathbf{1}\,[A(t) > A_{\text{th}}]\,dt}{\int_{\mathcal{V}} dt},$$
$$T_{\text{arr}} = t_{\text{arrival}} - t_{\text{push}}. \tag{21}$$

All conditions share A_{th}, windows, and validity rules. Missing observations are excluded from both exposure durations; undefined arrival is not replaced by the timeout. D, H use holding, and E_A, T_{arr} use pushing; approach and return are excluded.

Timestamp mappings align all streams to common trial time. Analysis uses a 2 s baseline before approach and a 3 s post-arrival hold. Each stem marker requires at least 90% coverage and no gap exceeding 0.15 s in both windows, without interpolation or filtering. Exposure uses $A_{\text{th}} = 0.65$ and requires at least 90% valid observed pushing time.

C. Branch-Like Contact-Cue Characterization

Three groups characterize the inputs and calculations of the controller, independently of the 384 plant-manipulation attempts. A1 contains six no-contact records (three stationary and three during robot motion) and 30 single-channel press–hold–release records: five repetitions per channel at robot TCP displacement commands of 0.5 and 1.0 mm against a rounded rigid tool centered on the channel. A2 contains seven single- and multiple-channel contact patterns with three repetitions each. A3 contains 12 changing-asymmetric-contact, static-contact, and release records. These 69 records use 20 Hz acquisition per channel; this sampling interval is not a contact-detection latency.

A1 references polarity-corrected capacitance to the first 2 s and averages 5.0–5.8 s. Across the six channel–input combinations, the coefficient of variation of five trial averages is 2.15–3.25% (Fig. 3(a)). Mean baseline standard deviations by channel and motion group are 0.007–0.014 pF. The median absolute post-release baseline offset (9.0–10.0 s) is 0.00475 pF across the 30 pressed-channel records.

A2 compares A and $\|\mathbf{q}_p\|$ over 5.3–5.8 s (Fig. 3(b)). With all channels pressed, their trial-averaged values are 0.682 and 0.052; single-channel resultant-to-maximum ratios are 0.975–0.977. Cancellation despite high individual responses supports retaining A independently for forward limiting.

A3 calculates $\omega_{\text{tac},n} = (\mathbf{e}_z^b)^\top \boldsymbol{\omega}_{\text{tac}}$ with $k_m = 0.2$ rad/s. Median RMS falls from 8.70×10^{-3} during changing contact (2.0–5.0 s) to 1.88×10^{-3} rad/s during static contact (5.3–7.5 s), with a median within-record reduction of 79.1% ($n = 12$). After release (9.0–10.0 s), the contact gate zeros the tactile term [Fig. 3(c)]. The RMS values describe the angular command. Section VI-D reports plant motion measured with stem markers.

D. Real-Plant Manipulation and Component Analysis

Fig. 4 and Table II summarize outcomes. Eligible observations are averaged within branches, then equally across all eight; standard deviations describe the eight branch means. D, H counts appear in Table I; E_A, T_{arr} use completed holds (92/91/96/90 for NT/IO/Trans/Full).

Mean displacement ranges from 14.99 to 15.70 mm. Trans has both the smallest displacement and the lowest holding variation: a quieter hold need not imply greater movement. Full has the largest descriptive displacement mean. Tactile conditions take longer and have higher above-threshold fractions than NT, showing that a commanded forward limit does not guarantee lower E_A.

Fig. 5 and Table III report paired contrasts. Full–NT is +0.398 mm, with an interval containing zero; Full–IO and Full–Trans are +0.547 and +0.595 mm, while Trans–IO is

Authorized licensed use limited to: CHONNAM NATIONAL UNIVERSITY. Downloaded on November 22,2026 at 10:55:00 UTC from IEEE Xplore. Restrictions apply.

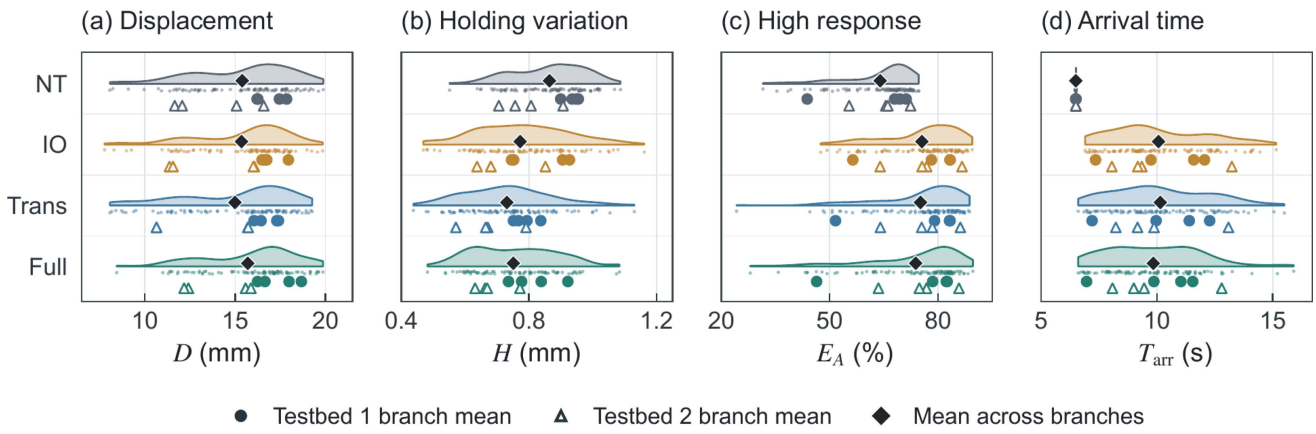


Fig. 4. Four-condition plant outcomes. Half-violins and small dots describe repeated-trial distributions. Circles and open triangles denote branch means in the two testbeds; black diamonds give the eight branches equal weight. Eligible counts for NT/IO/Trans/Full are 84/84/91/82 in (a,b) and 92/91/96/90 in (c,d). NT arrival times coincide and are shown as a line. Distributions are descriptive, not uncertainty intervals or independent plant samples.

TABLE II
REAL-PLANT OUTCOMES: MEAN ± STANDARD DEVIATION ACROSS EIGHT BRANCH MEANS

Condition	D [mm]	H [mm]	E_A [%]	T_{arr} [s]
No tactile (NT)	15.39 ± 2.34	0.864 ± 0.095	63.96 ± 9.68	6.50 ± 0.00
Intensity-only (IO)	15.35 ± 2.47	0.773 ± 0.110	75.52 ± 10.36	10.07 ± 2.04
Translation-only (Trans)	14.99 ± 2.75	0.731 ± 0.088	75.14 ± 11.68	10.15 ± 2.01
Proposed method (Full)	15.70 ± 2.34	0.751 ± 0.098	73.82 ± 12.99	9.84 ± 1.90

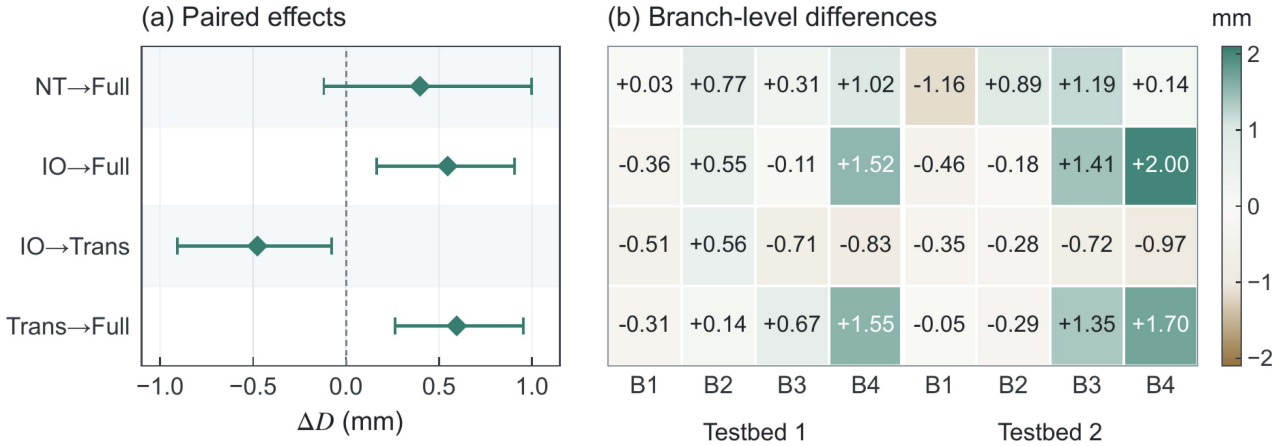


Fig. 5. Paired stem-displacement effects and branch-level differences from the same plant trials. Arrows run from reference to comparison; effects equal the arrow-head condition minus the arrow-tail condition. (a) Equal-weight branch-mean differences with descriptive conditional 95% intervals. (b) Paired mean differences for each selected branch in the two testbeds. Valid pair counts are 72, 70, 82, and 77 from top to bottom. The estimation and conditioning are specified in Section VI-E.

-0.477 mm. Full–IO is positive in four branches and negative in four, despite its positive mean. Full and Trans shared translational correction and intensity limiting, so their paired difference estimates the increment from enabling rotation with translation already active. To determine whether translation changes the effect of rotation, a rotation-only condition with the same intensity limit would be needed: its displacement difference from IO could then be compared with Full minus Trans.

Fig. 6 relates displacement to time and exposure on the same eligible pairs. Full–IO accompanies -0.343 s and -1.803 percentage points; Full–Trans accompanies -0.358 s and -1.536 percentage points. Full–NT instead accompanies +3.379 s and +10.212 percentage points. These joint outcomes describe costs and gains without identifying a time-adjusted causal mechanism.

E. Statistical Analysis

The 15 incomplete holds in Table I comprise eight timeouts, four sensor-related aborts, and three operator stops. Another 28

Authorized licensed use limited to: CHONNAM NATIONAL UNIVERSITY. Downloaded on November 22,2026 at 10:55:00 UTC from IEEE Xplore. Restrictions apply.

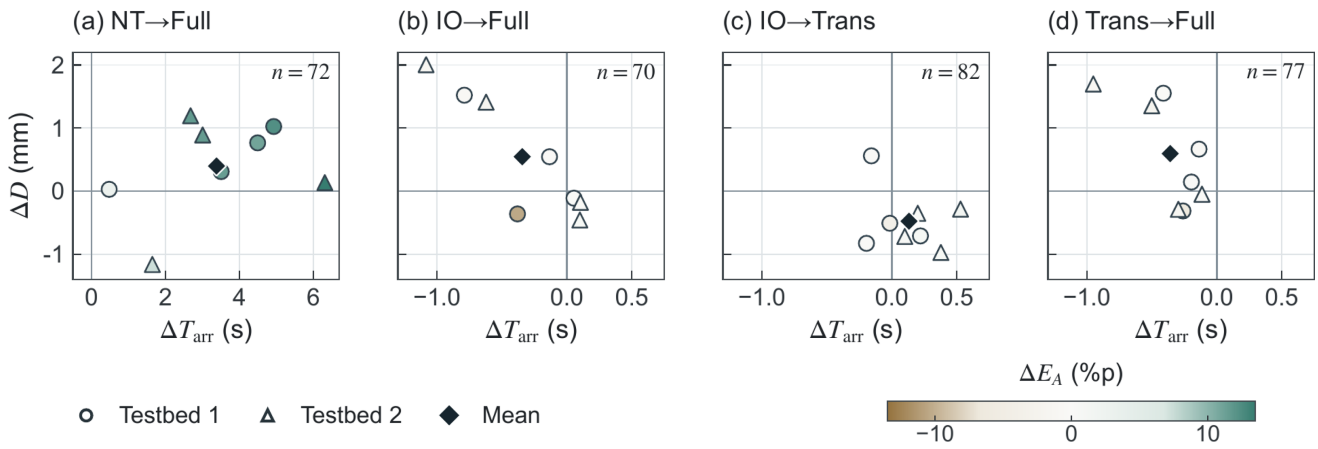


Fig. 6. Joint paired outcomes. Points show branch means; shapes denote testbeds and diamonds denote their equal-weight mean. Position encodes differences in arrival time and displacement; color encodes high-response exposure in percentage points (%p). Differences equal the arrow-head condition minus the arrow-tail condition. Panel (a) has a wider time axis than (b)–(d); displacement and color scales are shared. The same eligible pairs underlie all three differences within each contrast.

TABLE III
PAIRED STEM-DISPLACEMENT DIFFERENCES AND CONDITIONAL 95% INTERVALS

Contrast	$\widehat{\Delta}$ [mm]	95% interval [mm]	Pairs
Full–NT	+0.398	[-0.120, +0.999]	72
Full–IO	+0.547	[+0.165, +0.907]	70
Trans–IO	-0.477	[-0.906, -0.078]	82
Full–Trans	+0.595	[+0.264, +0.955]	77

completed holds lack eligible markers. Missing values remain undefined; terminal measurements from incomplete trials do not replace post-arrival outcomes. Holding results are conditional on completion and valid tracking, both of which can depend on execution.

Let D_{bka} denote displacement for branch b, repetition block k, and condition a. For a pair (a, c), $\mathcal{K}_b^{a,c}$ contains blocks with valid completed holds under both conditions. Each selected branch receives equal weight:

$$\widehat{\Delta}_{a,c} = \frac{1}{8}\sum_{b=1}^{8} \frac{1}{|\mathcal{K}_b^{a,c}|} \sum_{k\in\mathcal{K}_b^{a,c}} (D_{bka} - D_{bkc})\,. \qquad (22)$$

Contrast-specific eligible pairs need not reproduce differences between separately available condition means or add across contrasts. All summaries retain the same trial identifiers.

Conditional 95% intervals use percentile bounds of 4,000 bootstrap estimates (seed 20261704), fixing all eight branches. Within each branch, three consecutive four-block groups (1–4, 5–8, 9–12) are resampled with replacement, preserving internal order and missing entries. Sampling is independent across branches; valid-pair branch means and their equal-weight average are recomputed.

The procedure assumes exchangeable groups within branches, with only three groups available. It does not account for unmodeled cross-branch or session dependence, selection from incomplete execution or tracking loss, or plant-population uncertainty. Intervals are descriptive and nonsimultaneous; no confirmatory p values or significance claims are reported.

VII. DISCUSSION

The cue measurements explain why the controller assigns separate roles to peak intensity and the spatial resultant. Under simultaneous three-channel contact, opposing directions largely canceled in the resultant even though the peak remained high (Fig. 3(b)). Using the resultant alone to set forward speed would interpret that pattern as weak contact. The peak preserves the forward-speed limit in this case, while the resultant can still indicate the direction of asymmetric contact. The rate weighting addresses a different ambiguity: a sustained load can remain spatially asymmetric after it stops changing. The calculated angular correction subsided during the static hold (Fig. 3(c)). The contact tests measure how the cues respond to loading. In the plant trials, stem markers measure how far the branch moves under each controller.

The negative Trans–IO mean and the mixed branch-level Full–IO differences show that adding tactile corrections need not increase stem displacement. Arrival time also varied despite a shared TCP goal. Interpreting displacement alongside time and exposure distinguishes execution costs from stem motion; it does not identify the contact mechanics.

The full controller displaced the stem farther on average than intensity-only control and reached the same TCP goal sooner on their eligible paired trials (Fig. 6). Across the same eligible pairs, the mean differences were $+0.547$ mm in displacement and -0.343 s in arrival time. The displacement difference was negative on four branches, however, and the Full–NT displacement interval included zero. The data support a benefit relative to intensity-only slowing for the sampled branches on average; they leave open which contact geometries favor a correction on an individual branch.

Pruning-tool clearance depends on the cutting point, tool geometry, approach, and foliage envelope. The auxiliary arm must hold the stem through cutting and tool withdrawal

Authorized licensed use limited to: CHONNAM NATIONAL UNIVERSITY. Downloaded on November 22,2026 at 10:55:00 UTC from IEEE Xplore. Restrictions apply.

without obstructing the pruning arm. Coordinated planning must account for base placement, contact selection, compatible arm configurations, and collisions along feedback-modified paths. The approach–cut–release sequence remains untested.

The eight branches came from two plants. Stiffness, support, and contact location affect motion transmission; folding, sliding, and multiple contacts can change tactile cues. The trials did not vary stiffness, support, and contact location independently. Transfer to other canopies requires checking feasible references, calibration, gains, thresholds, and motion limits. Outdoor operation and field mounting remain unvalidated.

Force, torque, and crop damage limits require physical calibration and crop-specific testing. Automatic reference selection remains open. The plant trials compared four robot controllers; manual pruning served as the task motivation.

VIII. Conclusion

Three tactile channels guided translation and rotation while peak response limited forward speed. Across the sampled branches, Full–IO and Full–Trans had positive mean paired displacement differences, but branch-level effects varied and the Full–NT conditional interval included zero. Independent stem tracking showed how motion corrections affected the plant under a shared reference, alongside their effects on holding variation, tactile exposure, and execution time.

References

[1] K. O. Johnson, "The roles and functions of cutaneous mechanoreceptors," *Curr. Opin. Neurobiol.*, vol. 11, no. 4, pp. 455–461, 2001.

[2] R. S. Johansson and J. R. Flanagan, "Coding and use of tactile signals from the fingertips in object manipulation tasks," *Nature Rev. Neurosci.*, vol. 10, no. 5, pp. 345–359, 2009.

[3] A. W. Goodwin and H. E. Wheat, "Sensory signals in neural populations underlying tactile perception and manipulation," *Annu. Rev. Neurosci.*, vol. 27, pp. 53–77, 2004.

[4] Y. Park, J. Pak, C. Kim, and H. I. Son, "3D point cloud-based 6D pose estimation using the pedicel morphological features of fruits and vegetables," *Robot. Auton. Syst.*, vol. 194, 2025, Art. no. 105151.

[5] H. Yin et al., "Development, integration, and field evaluation of an autonomous citrus-harvesting robot," *J. Field Robot.*, vol. 40, no. 6, pp. 1363–1387, 2023.

[6] H. Zhou, X. Wang, W. Au, H. Kang, and C. Chen, "Intelligent robots for fruit harvesting: Recent developments and future challenges," *Precision Agriculture*, vol. 23, no. 5, pp. 1856–1907, 2022.

[7] N. H. Parayil, T. Peynot, and C. Lehnert, "RICE: Reactive interaction controller for cluttered canopy environment," in *Proc. IEEE Int. Conf. Robot. Automat.*, 2026, pp. 17406–17413.

[8] W. Mandil, V. Rajendran, K. Nazari, and A. Ghalamzan-Esfahani, "Tactile-sensing technologies: Trends, challenges and outlook in agri-food manipulation," *Sensors*, vol. 23, no. 17, 2023, Art. no. 7362.

[9] J. Seol et al., "Human-centered robotic system for agricultural applications: Design, development, and field evaluation," *Agriculture*, vol. 14, no. 11, 2024, Art. no. 1985.

[10] Y. Jo et al., "A review on dual-arm manipulation in agriculture," *IEEE Access*, vol. 13, pp. 150379–150399, 2025.

[11] K. Zhang, K. Lammers, P. Chu, Z. Li, and R. Lu, "An automated apple harvesting robot—From system design to field evaluation," *J. Field Robot.*, vol. 41, no. 7, pp. 2384–2400, 2024.

[12] J. Jun, J. Kim, J. Seol, J. Kim, and H. I. Son, "Towards an efficient tomato harvesting robot: 3D perception, manipulation, and end-effector," *IEEE Access*, vol. 9, pp. 17631–17 640, 2021.

[13] Y. Park, M.-S. Kim, J. Shin, Y. Cho, H.-J. Kim, and H. I. Son, "Autonomous self-propelled NAPA cabbage harvester: Cutting, attitude control, and loading modules," *Agriculture*, vol. 14, no. 11, 2024, Art. no. 1869.

[14] D. SepúLveda, R. Fernández, E. Navas, M. Armada, and P. González-De-Santos, "Robotic aubergine harvesting using dual-arm manipulation," *IEEE Access*, vol. 8, pp. 121889–121904, 2020.

[15] S. Stavridis, L. Droukas, and Z. Doulgeri, "Bimanual grape manipulation for human-inspired robotic harvesting," *IEEE/ASME Trans. Mechatron.*, vol. 30, no. 4, pp. 2722–2732, Aug. 2025.

[16] E. Gursoy, B. Navarro, A. Cosgun, D. Kulić, and A. Cherubini, "Towards vision-based dual arm robotic fruit harvesting," in *Proc. IEEE 19th Int. Conf. Automat. Sci. Eng.*, 2023, pp. 1–6.

[17] C. Lenz, R. Menon, M. Schreiber, M. P. Jacob, S. Behnke, and M. Bennewitz, "Hortibot: An adaptive multi-arm system for robotic horticulture of sweet peppers," in *Proc. IEEE/RSJ Int. Conf. Intell. Robots Syst.*, 2024, pp. 31–38.

[18] Y. Park and H. I. Son, "Visual scene understanding-based task planning for an efficient multipurpose agricultural robot system," *IEEE Robot. Automat. Lett.*, vol. 10, no. 12, pp. 13241–13248, Dec. 2025.

[19] W. E. Shaw-Cortez, D. Oetomo, C. Manzie, and P. Choong, "Tactile-based blind grasping: A discrete-time object manipulation controller for robotic hands," *IEEE Robot. Automat. Lett.*, vol. 3, no. 2, pp. 1064–1071, Apr. 2018.

[20] M. Matak and T. Hermans, "Planning visual-tactile precision grasps via complementary use of vision and touch," *IEEE Robot. Automat. Lett.*, vol. 8, no. 2, pp. 768–775, Feb. 2023.

[21] Y. Han et al., "Learning generalizable vision-tactile robotic grasping strategy for deformable objects via transformer," *IEEE/ASME Trans. Mechatron.*, vol. 30, no. 1, pp. 554–566, Feb. 2025.

[22] A. N. Chaudhury, T. Man, W. Yuan, and C. G. Atkeson, "Using collocated vision and tactile sensors for visual servoing and localization," *IEEE Robot. Automat. Lett.*, vol. 7, no. 2, pp. 3427–3434, Apr. 2022.

[23] N. F. Lepora, A. Church, C. de Kerckhove, R. Hadsell, and J. Lloyd, "From pixels to percepts: Highly robust edge perception and contour following using deep learning and an optical biomimetic tactile sensor," *IEEE Robot. Automat. Lett.*, vol. 4, no. 2, pp. 2101–2107, Apr. 2019.

[24] N. Vulin, S. Christen, S. Stevšić, and O. Hilliges, "Improved learning of robot manipulation tasks via tactile intrinsic motivation," *IEEE Robot. Automat. Lett.*, vol. 6, no. 2, pp. 2194–2201, Apr. 2021.

[25] M. Lambeta et al., "DIGIT: A novel design for a low-cost compact high-resolution tactile sensor with application to in-hand manipulation," *IEEE Robot. Automat. Lett.*, vol. 5, no. 3, pp. 3838–3845, Jul. 2020.

[26] L. Yang et al., "TacGNN: Learning tactile-based in-hand manipulation with a blind robot using hierarchical graph neural network," *IEEE Robot. Automat. Lett.*, vol. 8, no. 6, pp. 3605–3612, Jun. 2023.

[27] K.-W. Lee, Y. Qin, X. Wang, and S.-C. Lim, "DexTouch: Learning to seek and manipulate objects with tactile dexterity," *IEEE Robot. Automat. Lett.*, vol. 9, no. 12, pp. 10772–10779, Dec. 2024.

[28] Z. Zhao et al., "Tac-Man: Tactile-informed prior-free manipulation of articulated objects," *IEEE Trans. Robot.*, vol. 41, pp. 538–557, 2025.

[29] B. Xu et al., "Cushsense: Soft, stretchable, and comfortable tactile-sensing skin for physical human-robot interaction," in *Proc. IEEE Int. Conf. Robot. Automat.*, 2024, pp. 5694–5701.

[30] M. R. Dogar and S.S. Srinivasa, "A framework for push-grasping in clutter," in *Proc. Robot.: Sci. Syst. VII*, 2011, pp. 65–72.

[31] M. Stilman, J.-U. Schamburek, J. Kuffner, and T. Asfour, "Manipulation planning among movable obstacles," in *Proc. IEEE Int. Conf. Robot. Automat.*, 2007, pp. 3327–3332.

[32] Y. Park, C. Kim, and H. I. Son, "Fast and stable pedicel detection for robust visual servoing to harvest shaking fruits," *Comput. Electron. Agriculture*, vol. 220, 2024, Art. no. 108863.

[33] M. Danielczuk et al., "Mechanical search: Multi-step retrieval of a target object occluded by clutter," in *Proc. Int. Conf. Robot. Automat.*. IEEE, 2019, pp. 1614–1621.

[34] D. Brouwer et al., "Tactile-informed action primitives mitigate jamming in dense clutter," in *Proc. IEEE Int. Conf. Robot. Automat.*, IEEE, 2024, pp. 7991–7997.

[35] X. Zhang and S. Gupta, "Push past green: Learning to look behind plant foliage by moving it," in *Proc. 7th Conf. Robot Learn.*, vol. 229, 2023, pp. 3518–3535. [Online]. Available: https://proceedings.mlr.press/v229/zhang23k.html

Authorized licensed use limited to: CHONNAM NATIONAL UNIVERSITY. Downloaded on November 22,2026 at 10:55:00 UTC from IEEE Xplore. Restrictions apply.